Supporting Information

Two-dimensional perovskite solar cells with high luminescence and ultra-low open-circuit voltage deficit

Xiaomei Lian[a], Lijian Zuo[a]*, Haotian Wu[a], Guanqing Zhou[b], Chen Lin[b], Haiming Zhu[b], Gang Wu[a]*, David Cahen[c], Hongzheng Chen[a]*

[a]State Key Laboratory of Silicon Materials, MOE Key Laboratory of Macromolecular Synthesis and Functionalization, Department of Polymer Science and Engineering, Zhejiang University, Hangzhou 310027, P. R. China. E-mails: wmang@zju.edu.cn, zjuzlj@zju.edu.cn, hzchen@zju.edu.cn
[b] Department of Chemistry, Zhejiang University, Hangzhou 310027, P. R. China
[c] Bar Ilan Inst. for Nanotechn. & Adv. Materials, BINA & Chem. Dept., Bar Ilan Univ., Ramat Gan, 5290002, Israel

Experimental Section

Materials: Butylamine hydroiodide (BAI, 99%), phenylethyl-ammonium chlorine (PEACl, 99%), phenylethyl-ammonium iodide (PEAI, 99%), (6,6)-Phenyl-C_{61}-butyric acid methyl ester (PCBM, 99%), poly[bis(4-phenyl)(2,4,6-trimethylphenyl) amine](PTAA, M_w: 15000-25000) and PbI_2 (99%) were purchased from Xi'an Polymer. Bathocuproine (BCP, 99%) was purchased from TCI. Methylammonium iodide (MAI, 99%) was purchased from Shanghai Mater Win New Materials. N, N-dimethylformamide (DMF, 99%) was purchased from Alfa Aesar. Formamide (99.5%), chloroform (CF, 99%) and ethyl alcohol (99%) were ordered from Sigma Aldrich. Poly [(9,9-bis(3'-(N,NdiMethyl)-NethylaMMoiniuM-propyl)-2,7-fluorene)-alt-2,7-(9,9–dioctylfluorene)] dibroMide (PFN-Br, 99%) was purchased from Solarmer Materials Inc. All reagents and solvents were used directly if not specified.

Device fabrication and Characterization:

The ITO coated glass substrates were cleaned sequentially in detergent (Hellmanex III, 2 vol%), deionized water, acetone, and isopropanol in an ultrasonic bath for 15 min, respectively. After that, the substrates were dried in nitrogen flow and cleaned by UV-Ozone treatment for 20 min before use. PTAA HTL was prepared by spin-coating at 4000 rpm for 40 s, and then spin-coated PFN-Br atop of PTAA, followed by annealing at 100 °C for 10 min. BAI, PEACl (or PEAI), MAI, and PbI_2 were mixed by 1.8:0.2:3:4 molar ratio in DMF (with 3% formamide addition) with a concentration of 0.6M (based on PbI_2). The perovskite precursor solution and PTAA substrates were heated to 70 °C and 100 °C before the spin-coating of the perovskite layer. The spin-coating process started at 4000 rpm for 30 s after dropping the hot precursor to the preheated PTAA substrate, followed by annealing at 100 °C for 15 min. PCBM (5 mg/ml in CF) was spin-coated on the perovskite film at 2000 rpm for 30 s. BCP (0.5 mg/ml in ethyl alcohol) was then spin-coated on PCBM at 3000 rpm for 30 s, followed by a deposition of 100 nm Ag in a vacuum chamber under a high vacuum of 5×10^{-4} Pa. The heat-light co-treatment was carried out by annealing the device at temperature of 100 °C, with light intensity of 0.12 mW cm^{-2} for 48h.

The photocurrent density-voltage (*J-V*) measurement was performed via the solar simulator (SS-F5-3A, Enlitech) along with AM 1.5G spectra whose intensity was calibrated by the certified standard silicon solar cell (SRC-2020, Enlitech) at 100 mV cm^{-2}. The effective device pixel area in our case is 0.12 cm^2, while the devices were tested with an aperture of 0.06 cm^2. The external quantum efficiency (EQE) data were obtained by using the solar-cell spectral-response measurement system (QE-R, Enlitech). The perovskite solar cells were kept in a humidity-controlled cabinet (Hr = 50 ± 5%, Bossmen, PR1852(A)-SH) for humidity-stability measurement.

The UV-Visible absorption spectra were taken on UV-2450 UV-Vis Shimadzu Spectrophotometer, with the structure of ITO/PTAA/PFN-Br/$GA_{0.2}BA_{1.8}MA_5Pb_6I_{19}$/PCBM. The steady-state PL was taken on an FLSP920 from Edinburgh Instruments

and was excited by a Xenon lamp of 470 nm. Crystallographic properties of the perovskite films were investigated under Shimadzu XRD-7000 diffractometer with Cu K$_\alpha$ radiation of 0.15406 nm (graphite mono-chromatic) at a scanning rate of 10 $^\circ$ min^{-1}.

Transient absorption spectroscopy (TAS). For femtosecond transient absorption spectroscopy, the fundamental output from Yb:KGW laser (1030 nm, 220 fs Gaussian fit, 100 kHz, Light Conversion Ltd) was separated into two light beams. One was introduced to NOPA (ORPHEUS-N, Light Conversion Ltd) to produce a certain wavelength for pump beam (here we use 750 nm), the other was focused onto a YAG plate to generate white light continuum as the probe beam. The pump and probe overlapped on the sample at a small angle less than 10°. The transmitted probe light from the sample was collected by a linear CCD array. Then we obtained transient differential transmission signals by the equation shown below:

$$\frac{\Delta T}{T} = \frac{T_{pump-on} - T_{pump-off}}{T_{pump-off}}$$

(1)

We follow Jin's and Sargent's work (J. Phys. Chem. Lett. 2019, 10, 419-426, J. Am. Chem. Soc. 2017, 139, 1432-1435) to quantify the charge transfer time. In more detail, we consider the rising part of TA kinetics (Figure 3c, f, i) as a charge transfer process, and a single exponential fitting model is used here to extract charge transfer time.

Transient photovoltage (TPV) measurements: In TPV measurements, the device was held at opencircuit under steady-state conditions controlled by a continuous white light bias and a small pulsed perturbation of excess charge carriers produced by alaser beam (470 nm). The device connected to the oscilloscope (1M Ω input impedance). The lifetime (τ) was calculated by fitting a single exponential function to the transient photovoltage or transient photocurrent decay curves.

Bilayer hole-only devices characterization (SCLC). SCLC was carried out for the hole-only device, with the structure of ITO/PTAA/PFN-Br/GA$_{0.2}$BA$_{1.8}$MA$_5$Pb$_6$I$_{19}$/PTAA/MoO$_3$/Ag. The defect density could be calculated by the Mott-Gurney law:

$$J = \frac{9}{8}\varepsilon_r\varepsilon_0\mu\frac{V^2}{L^3}$$

(2)

Here, ε and ε_0 are the dielectric constants of perovskite and the vacuum permittivity, respectively. L is the thickness of the obtained perovskite film, about 300 nm in this study. e is the elementary charge, and V_{TFL} is the trap-filled limit voltage. When ε is constant, $N_{defects}$ is in direct proportion to V_{TFL}.

Time-of-flight secondary-ion mass spectrometry (TOF-SIMS). The TOF-SIMS spectra were conducted on a TOF-SIMS V instrument (Ion-TOF, GmbH, Germany) to track the depth distributions of Cl$^-$, and I$^-$ and In^{3+} from the top of perovskite film down to ITO substrate. Dual beam depth profiling used a pulsed 30keV Bi$_3^{++}$ liquid metal ion gun as a primary ion source and a 10 keV Argon gas cluster ion beam with the beam current being lowered to 1 nA as a sputtering ion source in an interlaced mode. At first, the sputter beam was used to sputter the sample surface for 20 s to clean possible contamination on the sample surface during sample preparation. Then, data were collected until we reached the ITO layer as indicated by the sharp increase in the InO$^-$ ion intensity. The analysis area was 100×100 μm^2 in the center of a crater of 300×300 μm^2. A low energy flood gun was used for charge compensation during analysis. The spectra were obtained in a high current bunched mode and mass calibrated using Cl$^-$, and I$^-$ and InO$^-$. The amount and distribution of Cl$^-$ (I$^-$) inside the perovskite layer can be illustrated by the relative intensity of Cl$^-$ (I$^-$), until the enhancement of the relative intensity of InO$^-$ signal. All geometries of intermediates were optimized under tight criteria using BHandH/6-31G(d,p) method. Frequency calculations confirmed that the intermediates on ground state had zero imaginary frequency. All calculations were performed using Gaussian 16 program software.
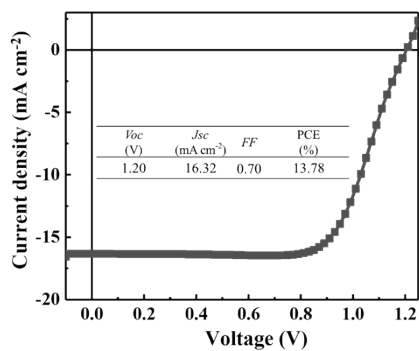
Figure S1. *J-V* curve and photovoltaic parameters of the $BA_2MA_3Pb_4I_{13}$ based device after heat-light co-treatment.
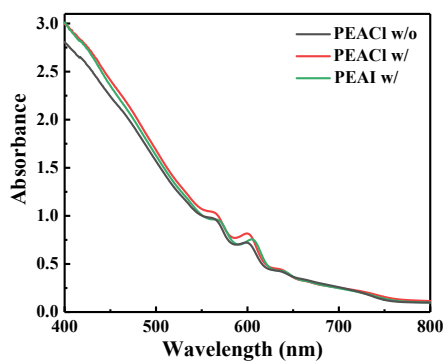

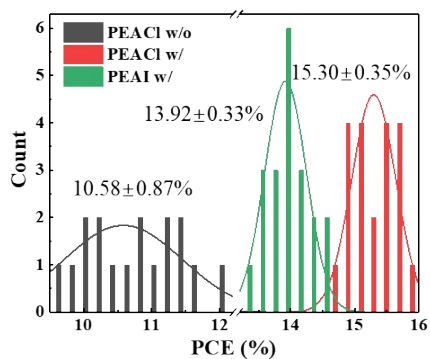**Figure S2.** UV-Vis absorption spectra of the PEACl w/o, PEACl w/, and PEAI w/ -based perovskite films.

Figure S3. PCE histograms of 20 devices of the PEACl w/o, PEACl w/, and PEAI w/ -based PVSCs.
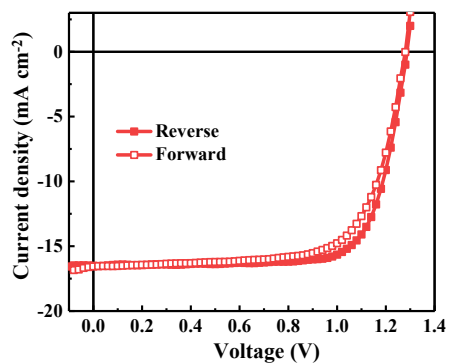
Figure S4. The forward-reverse *J-V* curves of the PEACl w/ -based champion PVSC.
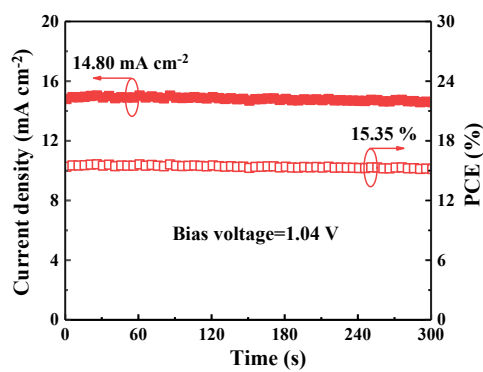

Figure S5. Stabilized photocurrent measurement of the PEACl w/ -based champion PVSC under 1 sun AM 1.5G continuous illumination.
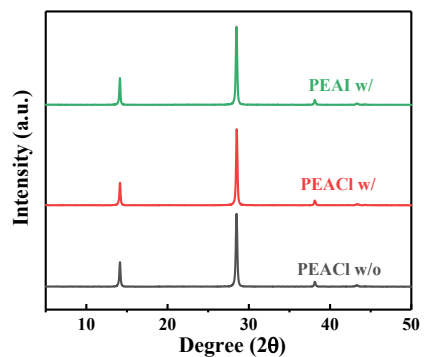

Figure S6. XRD patterns of PEACl w/o, PEACl w/, and PEAI w/ -based perovskite films, using CuK$_\alpha$ X-radiation.
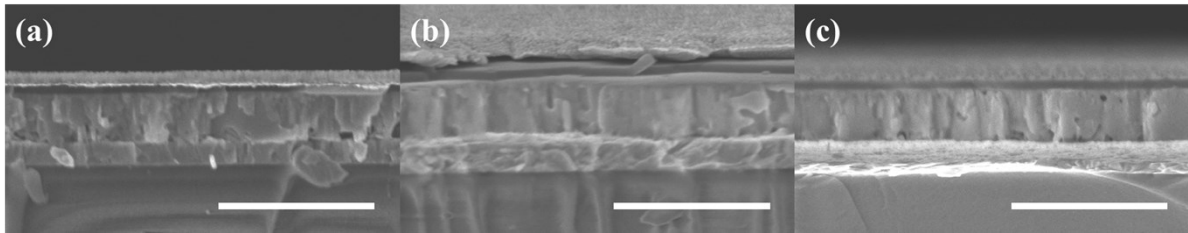
Figure S7. The top-view SEM images of the (a) PEACl w/o, (b) PEACl w/ and (c) PEAI w/ perovskite films (The scale bar is 1 mm).
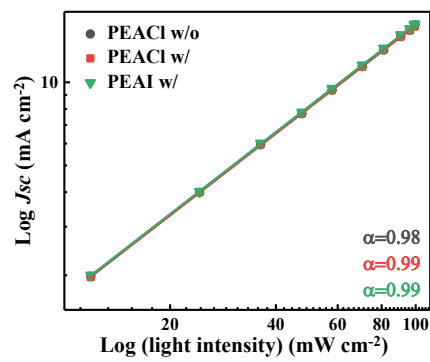

Figure S8. LogJsc vs. Log(light intensity) (dots), together with linear fits (solid lines) to the data, for the PEACl w/o, PEACl w/, and PEAI w/ -based devices.

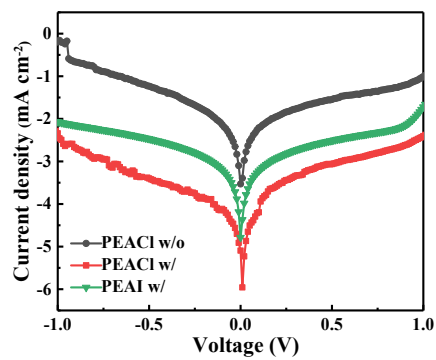**Figure S9.** J-V curves in the dark of the PEACl w/o, PEACl w/, and PEAI w/ -based PVSCs.
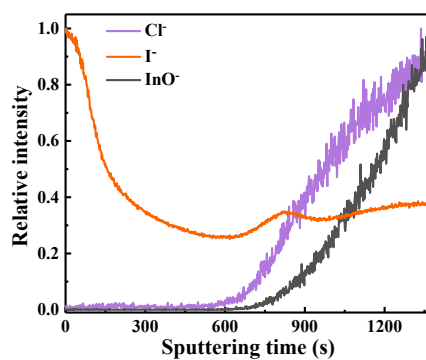
Figure S10. TOF-SIMS profiles showing Cl$^-$, and I$^-$ of the PEA$_{0.2}$BA$_{1.8}$MA$_3$Pb$_4$I$_{13}$ films from the top of the perovskite film to the bottom for the PEACl w/ based perovskite film.
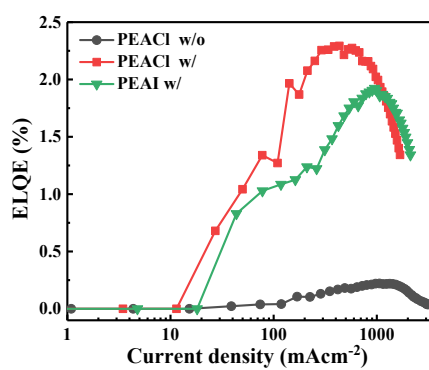

Figure S11. ELQE as a function of injection current density for the PEACl w/o, PEACl w/, and PEAI w/ -based devices

Table S1. Reported quasi-2D PVSCs with high *Voc.*

Voc (V)	Jsc (mA cm^{-2})	FF	PCE (%)	Eg [a] (eV)	Energy loss (V)	Ref
1.24	19.86	0.70	17.26	1.69	0.45	1
1.16	19.00	0.79	17.34	1.61	0.45	2
1.22	17.91	0.82	18.04	1.65	0.43	3
1.17	16.90	0.81	15.86	1.66	0.49	4
1.23	13.61	0.72	12.07	1.68	0.45	5
1.19	15.80	0.75	14.10	1.64	0.45	6
1.13	18.63	0.77	16.26	1.62	0.49	7
1.14	22.26	0.73	18.48	1.64	0.50	8
1.07	19.55	0.75	15.75	1.61	0.54	9
1.23	15.85	0.75	14.68	1.68	0.45	10
1.09	21.77	0.75	18.06	1.61	0.52	11
1.24	20.89	0.66	17.25	1.62	0.38	12
1.21	17.97	0.76	16.53	1.68	0.47	13
1.29	16.51	0.74	15.81	1.65	0.36	This work

a) The bandgap is calculated according to the PL spectra.

Table S2. Summary of the photovoltaic parameters of the PEACl w/o, PEAI w/o, PEACl w/, and PEAI w/ -based PVSCs.

	Voc$_{ave}$ (V)	PCE$_{ave}$ (%)	Jcal (mA cm^{-2})
PEACl w/o	1.16±0.02	10.58±0.87	14.43
PEAI w/o	1.15±0.02	10.72±0.65	14.42
PEACl w/	1.28±0.01	15.30±0.35	16.49
PEAI w/	1.24±0.01	13.92±0.33	16.06

Table S3. The forward-reverse *J-V* character of the PEACl w/ -based champion PVSC.

	Voc (V)	FF	Jsc (mA cm^{-2})	PCE (%)	HI (%)
Reverse	1.29	0.74	16.51	15.81	6.3
Forward	1.28	0.70	16.56	14.81	

Table S4. The charge transfer time of small-n to large-n of the PEACl w/o, PEACl w/, and PEAI w/ -based perovskite films, derived by fitting the carrier dynamics via a single exponential equation.

Sample	PEACl w/o (ps)	PEACl w/ (ps)	PEAI w/ (ps)
n=2 → n=3	0.40±0.01	0.30±0.04	0.29±0.01
n=3 → n=4	0.48±0.01	0.48±0.03	0.40±0.04
Small → n= ∞	60.87±5.35	28.43±2.99	28.41±4.60

Table S5. Comparison of experimental XRD data for two characteristic peaks of the PEACl w/o, PEACl w/, and PEAI w/ - based perovskite films.

Ratio	Plane	(111) (14.1°)	(202) (28.4°)
PEACl w/o	FWHM (°)	0.172	0.209
	Intensity (cps)	2.9×10^4	8.5×10^4
PEACl w/	FWHM (°)	0.184	0.203
	Intensity (cps)	2.3×10^4	8.9×10^4
PEAI w/	FWHM (°)	0.187	0.228
	Intensity (cps)	2.6×10^4	8.0×10^4

Table S6. Carrier recombination lifetime of the PEACl w/o, PEACl w/, and PEAI w/ based devices.

Sample	PEACl w/o	PEACl w/	PEAI w/
Lifetime (μs)	2.62±0.02	3.02±0.03	2.84±0.03

References

1   G. Wu, X. Li, J. Zhou, J. Zhang, X. Zhang, X. Leng, P. Wang, M. Chen, D. Zhang, K. Zhao, S. F. Liu, H. Zhou and Y. Zhang, *Adv. Mater.*, 2019, **31**, 1903889.

2   J. Shi, Y. Gao, X. Gao, Y. Zhang, J. Zhang, X. Jing and M. Shao, *Adv. Mater.*, 2019, **31**, 1901673.

3   J. Zhang, J. J. Qin, M. S. Wang, Y. J. Bai, H. Zou, J. K. Keum, R. M. Tao, H. X. Xu, H. M. Yu, S. Haacke and B. Hu, *Joule*, 2019, **3**, 3061-3071.

4   X. Lian, J. Chen, Y. Zhang, S. Tian, M. Qin, J. Li, T. R. Andersen, G. Wu, X. Lu and H. Chen, *J. Mater. Chem. A*, 2019, **7**, 18980-18986.

5   J. Chen, X. Lian, Y. Zhang, W. Yang, J. Li, M. Qin, X. Lu, G. Wu and H. Chen, *J. Mater. Chem. A*, 2018, **6**, 18010-18017.

6   W. F. Fu, J. Wang, L. J. Zuo, K. Gao, F. Liu, D. S. Ginger and A. K. Y. Jen, *ACS Energy Lett.*, 2018, **3**, 2086-2093.

7   X. Lian, J. Chen, Y. Zhang, M. Qin, T. R. Andersen, J. Ling, G. Wu, X. Lu, D. Yang and H. Chen, *J. Mater. Chem. A*, 2019, **7**,

19423-19429.

8   T. Luo, Y. Zhang, Z. Xu, T. Niu, J. Wen, J. Lu, S. Jin, S. F. Liu and K. Zhao, *Adv. Mater.*, 2019, **31**, 1903848.

9   D. Lu, G. Lv, Z. Xu, Y. Dong, X. Ji and Y. Liu, *J. Am. Chem. Soc.*, 2020, **142**, 11114-11122.

10 Y. Qin, H. Zhong, J. J. Intemann, S. Leng, M. Cui, C. Qin, M. Xiong, F. Liu, A. K. Y. Jen and K. Yao, *Adv. Energy Mater.*, 2020, **10**, 1904050.

11 H. Ren, S. Yu, L. Chao, Y. Xia, Y. Sun, S. Zuo, F. Li, T. Niu, Y. Yang, H. Ju, B. Li, H. Du, X. Gao, J. Zhang, J. Wang, L. Zhang, Y. Chen and W. Huang, *Nat. Photonics*, 2020, 14, 154-163.

12 Z. Xu, D. Lu, F. Liu, H. Lai, X. Wan, X. Zhang, Y. Liu and Y. Chen, *ACS Nano*, 2020, 14, 4871-4881.

13 T. He, S. Li, Y. Jiang, C. Qin, M. Cui, L. Qiao, H. Xu, J. Yang, R. Long, H. Wang and M. Yuan, *Nat. Commun.*, 2020, 11, 1672.